Gamow-Teller strength distributions in ^{76}Ge and ^{76}Se from deformed quasiparticle random-phase approximation

P. Sarriguren and E. Moya de Guerra

Instituto de Estructura de la Materia, Consejo Superior de Investigaciones Científicas, Serrano 123, E-28006 Madrid, Spain

L. Pacearescu and Amand Faessler

Institute für Theoretische Physik, Universität Tübingen, D-72076 Tübingen, Germany

F. Šimkovic

Department of Nuclear Physics, Comenius University, SK-842 15 Bratislava, Slovakia

A. A. Raduta

*Department of Theoretical Physics and Mathematics, Bucharest University, Bucharest, P.O. Box MG11, Romania
and Institute of Physics and Nuclear Engineering, Bucharest, P.O. Box MG6, Romania*

We study Gamow-Teller strength distributions of ^{76}Ge and ^{76}Se within a deformed quasiparticle random-phase approximation formalism, which includes residual spin-isospin forces in the particle-hole and particle-particle channels. We consider two different methods to construct the quasiparticle basis, a self-consistent approach based on a deformed Hartree-Fock calculation with density-dependent Skyrme forces and a more phenomenological approach based on a deformed Woods-Saxon potential. Both methods contain pairing correlations in the BCS approach. We discuss the sensitivity of Gamow-Teller strength distributions to the deformed mean field and residual interactions.

I. INTRODUCTION

The nuclear double β-decay process is widely considered [1] as one of the most important sources of information about fundamental issues, such as lepton number nonconservation and massive neutrinos, that can be used to test the standard model.

Theoretically, a condition to obtain reliable estimates for the limits of the double β-decay half-lives is that the nuclear structure involved in the process through the nuclear matrix elements can be calculated correctly. The proton-neutron quasiparticle random-phase approximation (pnQRPA or QRPA in short) is one of the most reliable and extended microscopic approximations for calculating the correlated wave functions involved in β and double β-decay processes. The method was first studied in Ref. [2] to describe the β strength. It was developed on spherical single-particle wave functions and energies with pairing and residual interactions.

The QRPA method was also successfully applied to the description of double β decay [3] after the inclusion of a particle-particle (pp) residual interaction, in addition to the particle-hole (ph) usual channel. Many more extensions of the QRPA method have been proposed in the literature, see Ref. [4] and references therein.

An extension of the pnQRPA method to deal with deformed nuclei was done in Ref. [5], where a Nilsson potential was used to generate single-particle orbitals. Subsequent extensions including Woods-Saxon (WS) type potentials [6], residual interactions in the particle-particle channel [7], self-consistent deformed Hartree-Fock (HF) mean fields with consistent residual interactions [8], and self-consistent approaches in spherical neutron-rich nuclei [9], can also be found in the literature. Nevertheless, the effect of deformation on the double β-decay processes has not been sufficiently studied [10,11].

In Ref. [8], ground state and β-decay properties of exotic nuclei were studied on the basis of a deformed self-consistent HF+BCS+QRPA calculation with density dependent effective interactions of Skyrme type. This is a well-founded approach that has been very successful in the description of spherical and deformed nuclei within the valley of stability [12]. In this work we extend those calculations to the study of the dependence on deformation of the single β branches that build up the double β process. We focus on the example of the double β decay of ^{76}Ge and study β^- Gamow-Teller (GT) transitions to the intermediate nucleus as well as the β^+ Gamow-Teller transitions of the daughter nucleus ^{76}Se to the same intermediate nucleus. We discuss the similarities and differences of using different single-particle mean fields of WS and HF types.

In Sec. II, we present a brief summary containing the basic points in our theoretical description. Section III contains the results obtained for the bulk properties of ^{76}Ge and ^{76}Se and a comparison of our results with the experimental available information. In Sec. IV we present our results for the GT strength distributions and discuss their dependence on the deformed mean field and residual interactions. The conclusions are given in Sec. V.

II. THEORETICAL APPROACH

In this section we describe the QRPA formalism used in this work, which is based on two different assumptions for the deformed mean field, a Woods-Saxon potential and a

self-consistent mean field obtained from a Hartree-Fock procedure with Skyrme forces.

In the first approach we use a deformed WS potential with axial symmetry to generate single-particle energies and wave functions. The parameters of this potential are taken from the work of Tanaka *et al.* [13]. This parametrization was proposed originally for spherical nuclei ranging from ^{16}O to ^{208}Pb, but the derived isospin dependence of the parameters allows an extension to deformed nuclei as well. Previous QRPA calculations have shown that this parametrization provides realistic levels also for deformed nuclei and good results on $M1$ excitations were obtained [14] for nuclei in various mass regions as well.

In these calculations, the quadrupole deformation of the WS potential β_2 is usually determined by fitting the microscopically calculated ground state quadrupole moment to the corresponding experimental value. The hexadecapole deformation β_4 is expected to be small for these nuclei and we assume it is equal to zero.

On the other hand, we also perform self-consistent microscopic calculations based on a deformed HF method with density-dependent Skyrme interactions. We consider in this paper the force Sk3 [15] and the force SG2 [16] that has been successfully tested against spin and isospin excitations in spherical [16] and deformed nuclei [8,17]. For the solution of the HF equations we follow the McMaster procedure that is based on the formalism developed in Ref. [18], as described in Ref. [19]. Time reversal and axial symmetry are also assumed here.

In both schemes, WS and HF, the single-particle wave functions are expanded in terms of the eigenstates of an axially symmetric harmonic oscillator in cylindrical coordinates, which are written in terms of Laguerre and Hermite polynomials. The single-particle states $|i\rangle$ and their time reversed $|\bar{i}\rangle$ are characterized by the eigenvalues Ω of J_z, parity π_i, and energy ϵ_i,

$$|i\rangle = \sum_N \frac{(-1)^N + \pi_i}{2} \sum_{n_r,n_z,\Lambda \geq 0, \Sigma} C^i_{N n_r n_z \Lambda \Sigma} |N n_r n_z \Lambda \Sigma\rangle$$

(1)

with $\Omega_i = \Lambda + \Sigma \geq \frac{1}{2}$, and

$$|\bar{i}\rangle = \sum_N \frac{(-1)^N + \pi_i}{2} \sum_{n_r,n_z,\Lambda \geq 0, \Sigma} C^i_{N n_r n_z \Lambda \Sigma} (-1)^{1/2 - \Sigma}$$
$$\times |N n_r n_z - \Lambda - \Sigma\rangle$$

(2)

with $\Omega_{\bar{i}} = -\Omega_i = -\Lambda - \Sigma \leq -\frac{1}{2}$. For each N the sum over $n_r, n_z, \Lambda \geq 0$ is extended to the quantum numbers satisfying $2n_r + n_z + \Lambda = N$. The sum over N goes from $N = 0$ to $N = 10$ in our calculations.

Pairing correlations between like nucleons are included in both cases in the BCS approximation with fixed gap parameters for protons Δ_π, and neutrons Δ_ν.

The number equation in the neutron sector reads

$$2 \sum_i v_i^2 = N,$$

(3)

where v_i^2 are the occupation probabilities

$$v_i^2 = \frac{1}{2} \left[1 - \frac{\epsilon_i - \lambda_\nu}{E_i} \right], \quad u_i^2 = 1 - v_i^2$$

(4)

in terms of the quasiparticle energies

$$E_i = \sqrt{(\epsilon_i - \lambda_\nu)^2 + \Delta_\nu^2}.$$

(5)

These equations are solved iteratively for the WS and HF single-particle energies to determine the Fermi level λ_ν and the occupation probabilities. Similar equations are used to determine the Fermi level and occupation probabilities for protons by changing N into Z, Δ_ν into Δ_π, and λ_ν into λ_π.

The fixed gap parameters are determined phenomenologically from the odd-even mass differences through a symmetric five term formula involving the experimental binding energies [20],

$$\Delta_\nu = \frac{1}{8} [B(N-2,Z) - 4B(N-1,Z) + 6B(N,Z)$$
$$- 4B(N+1,Z) + B(N+2,Z)].$$

(6)

A similar expression is found for the proton gap Δ_π by changing N by Z and vice versa. For ^{76}Ge we obtain $\Delta_\nu = 1.54$ MeV, $\Delta_\pi = 1.56$ MeV and for ^{76}Se we obtain $\Delta_\nu = 1.71$ MeV and $\Delta_\pi = 1.75$ MeV.

Therefore, at the quasiparticle mean field level, we can observe several differences with respect to the treatment of the mean field in terms of HF or WS potential. The most important is that the quadrupole deformation of the ground state is determined self-consistently in HF and no explicit input parameter is needed. Other differences come from the structure of the two-body density-dependent Skyrme force that contains terms absent in the WS potential, such as a spin-spin interaction in the self-consistent mean field through the spin exchange operators of the Skyrme force.

Now, we add to the mean field a spin-isospin residual interaction, which is expected to be the most important residual interaction to describe GT transitions. This interaction contains two parts. A particle-hole part, which is responsible for the position and structure of the GT resonance [7,8] and a particle-particle part, which is a neutron-proton pairing force in the $J^\pi = 1^+$ coupling channel,

$$V^{ph}_{GT} = 2\chi^{ph}_{GT} \sum_{K=0,\pm 1} (-1)^K \beta^+_K \beta^-_{-K},$$

$$\beta^+_K = \sum_{\pi\nu} \langle \nu | \sigma_K | \pi \rangle a^+_\nu a_\pi,$$

(7)

$$V^{pp}_{GT} = -2\kappa^{pp}_{GT} \sum_K (-1)^K P^+_K P_{-K},$$

$$P^+_K = \sum_{\pi\nu} \langle \pi | (\sigma_K)^+ | \nu \rangle a^+_\nu a^+_{\bar{\pi}}.$$

(8)

The two forces ph and pp are defined with a positive and a negative sign, respectively, according to their repulsive and attractive character, so that the coupling strengths χ and κ take positive values.

The particle-hole residual interaction could, in principle, be obtained consistently from the same Skyrme force used to create the mean field as was done in Ref. [8] to study exotic nuclei. However, in this paper we use as a first attempt the coupling strengths from Ref. [7]. In this reference, the strengths χ_{GT}^{ph}, and κ_{GT}^{pp} are considered to be smooth functions of the mass number A, proportional to A^μ. The strength of the ph force is determined by adjusting the calculated positions of the GT giant resonances for ^{48}Ca, ^{90}Zr, and ^{208}Pb. This gives a mass dependence with $\mu=0.7$. The same mass dependence is assumed for the pp force and the coefficient is determined by a fitting procedure to β-decay half-lives of nuclei with $Z\leqslant40$. The result found in Ref. [7] is $\chi_{GT}^{ph}=5.2/A^{0.7}$ MeV and $\kappa_{GT}^{pp}=0.58/A^{0.7}$ MeV. A word of caution is in order concerning this parametrization of the residual forces. It serves to our purpose of comparing the effects of different deformed mean fields on the GT strength distributions, but one should keep in mind that the coupling strengths obtained in this way depend, in particular, on the model used for single-particle wave functions and on the set of experimental data considered. In Ref. [7] a Nilsson potential was used and the set of experimental data did not include the nuclei under study here. Therefore, the coupling strengths of Ref. [7] cannot be safely extrapolated and are not necessarily the best possible choices. As we shall see in the following sections, the strengths from Ref. [7] reproduce well the data when using the WS potential, but one needs a somewhat smaller value of χ_{GT}^{ph} to reproduce the GT resonance with the HF mean field.

The proton-neutron quasiparticle random-phase approximation phonon operator for GT excitations in even-even nuclei is written as

$$\Gamma_{\omega_K}^+ = \sum_{\pi\nu} [X_{\pi\nu}^{\omega_K}\alpha_\nu^+\alpha_{\bar\pi}^+ + Y_{\pi\nu}^{\omega_K}\alpha_{\bar\nu}\alpha_\pi], \qquad (9)$$

where $\alpha^+(\alpha)$ are quasiparticle creation (annihilation) operators, ω_K are the RPA excitation energies, and $X_{\pi\nu}^{\omega_K}, Y_{\pi\nu}^{\omega_K}$ the forward and backward amplitudes, respectively. The solution of the QRPA equations can be found solving first a dispersion relation [21], which is of fourth order in the excitation energies ω_K.

In the intrinsic frame the GT transition amplitudes connecting the QRPA ground state $|0\rangle(\Gamma_{\omega_K}|0\rangle=0)$ to one phonon states $|\omega_K\rangle(\Gamma_{\omega_K}^+|0\rangle=|\omega_K\rangle)$, are given by

$$\langle\omega_K|\sigma_K t^\pm|0\rangle = \mp M_\pm^{\omega_K}. \qquad (10)$$

The functions $M_\pm^{\omega_K}$ can be found, for instance, in Ref. [21]. The basic ingredients in their structure are the spin matrix elements connecting neutron and proton states with spin operators

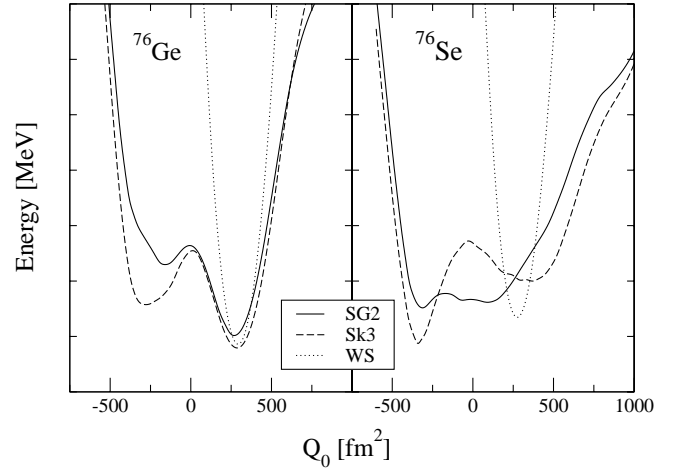$$\Sigma_K^{\nu\pi} = \langle\nu|\sigma_K|\pi\rangle, \qquad (11)$$

FIG. 1. Total energy as a function of the mass quadrupole moment obtained from deformed Hartree-Fock calculations with the Skyrme forces SG2 (solid line) and Sk3 (dashed lines), and from deformed Woods-Saxon potentials (dotted line). The origin of the energy axis is different in each case but the distance between ticks corresponds always to 1 MeV.

which can be written in terms of the coefficients of the expansion in Eqs. (1) and (2),

$$\Sigma_K^{\nu\pi} = \sum_{Nn_z\Lambda\Sigma} C_{Nn_z\Lambda\Sigma+K}^\nu C_{Nn_z\Lambda\Sigma}^\pi (2\Sigma)\sqrt{1+|K|}, \qquad (12)$$

$$\Sigma_{K=1}^{\nu\bar\pi} = \sum_{Nn_z} C_{Nn_z01/2}^\nu C_{Nn_z01/2}^\pi (-\sqrt{2}). \qquad (13)$$

Once the intrinsic amplitudes are calculated according to Eq. (10), the GT strength $B(GT)_\pm$ in the laboratory system for a transition $I_iK_i(0^+0)\to I_fK_f(1^+K_f)$ can be obtained as

$$B(GT)_\pm = \frac{g_A^2}{4\pi} [\delta_{K_f,0}\langle\phi_{K_f}|\sigma_0 t^\pm|\phi_0\rangle^2 + 2\delta_{K_f,1}\langle\phi_{K_f}|\sigma_1 t^\pm|\phi_0\rangle^2], \qquad (14)$$

where we have used the initial and final states in the laboratory frame expressed in terms of the intrinsic states $|\phi_K\rangle$ using the Bohr-Mottelson factorization [22].

In the simple uncorrelated two-quasiparticle (2qp) approximation, neglecting the residual ph and pp forces, the functions $M_\pm^{\omega_K}$ reduce to the following expressions:

$$M_+^{\omega_K} = u_\nu v_\pi \Sigma_K^{\nu\pi}, \qquad M_-^{\omega_K} = v_\nu u_\pi \Sigma_K^{\nu\pi}, \qquad (15)$$

where the excitation energies are the bare two quasiparticle energies $\omega_K^{2qp}=E_\nu+E_\pi$.

The Ikeda sum rule is always fulfilled in our calculations,

$$\sum_\omega [(M_-^\omega)^2 - (M_+^\omega)^2] = 3(N-Z). \qquad (16)$$

TABLE I. Charge root mean square radii r_c (fm), intrinsic charge quadrupole moments Q_p (fm^2), and quadrupole deformations β for ^{76}Ge and ^{76}Se calculated with various assumptions for the mean field. In the case of ^{76}Se we show theoretical values corresponding to the prolate shape in first place and to the oblate shape in second place. Experimental values for r_c are from Ref. [24] and for Q_p from Ref. [26] the first value and from Ref. [27] the second (see text).

		r_c	Q_p	β
^{76}Ge	Expt.	4.080–4.127	66(21)–164(24)	0.10–0.24
	Sk3	4.130	111.0	0.161
	SG2	4.083	105.9	0.157
	WS	3.950	110.9	0.176
^{76}Se	Expt.	4.088–4.162	119(25)–205(24)	0.16–0.29
	Prolate/oblate	Prolate/oblate	Prolate/oblate	Prolate/oblate
	Sk3	4.170/4.180	117.5/−136.0	0.158/−0.181
	SG2	4.113/4.143	35.2/−140.6	0.049/−0.191
	WS	3.991/4.138	81.6/−141.4	0.119/−0.193

III. BULK PROPERTIES

In this section we present results for the bulk properties of ^{76}Ge and ^{76}Se obtained from WS and HF descriptions.

First, we analyze the energy surfaces as a function of deformation. In the case of WS, this is simply done by varying the quadrupole deformation of the potential β_2, which is an input parameter. In the case of HF, we perform constrained calculations [23], minimizing the HF energy under the constraint of keeping fixed the nuclear deformation.

We can see in Fig. 1 the total energy plotted versus the microscopically calculated mass quadrupole moment. The results correspond to HF calculations with the forces SG2 (solid line) and Sk3 (dashed line), as well as to calculations with the WS potential (dotted line). The origin of the energy axis is different in each case but the distance between ticks corresponds always to 1 MeV.

We observe that the HF calculation predicts the existence of two energy minima close in energy, giving rise to shape isomers in these nuclei, while the WS potential originates a single energy minimum, which is in agreement with the absolute prolate minimum in the case of ^{76}Ge and close to the prolate HF solution in the case of ^{76}Se.

We can see in Table I the experimental and the microscopically calculated charge root mean square radii r_c, quadrupole moments Q_p, and quadrupole deformations β ($\beta = \sqrt{\pi/5}\, Q_p / Z r_c^2$). In the case of ^{76}Se, the calculated values correspond to prolate/oblate deformations. The input WS prolate deformation is chosen to be $\beta_2 = 0.10$ in both nuclei ^{76}Ge and ^{76}Se. In the oblate case of the nucleus ^{76}Se, the WS deformation chosen is $\beta_2 = -0.20$. With these values we guarantee that the intrinsic deformations of the ground state are similar in HF and WS and therefore the differences in their predictions will have their origin in the structure of mean fields having the same deformation.

The values obtained for the charge radii are in good agreement with the experimental values from Ref. [24], which are also shown in Table I. They are also in good agree-

ment with the results obtained from relativistic mean field calculations [25]: $r_{c(\text{rel})}(^{76}\text{Ge}) = 4.057$ fm and $r_{c(\text{rel})}(^{76}\text{Se}) = 4.119$ fm.

The charge quadrupole moments quoted in Table I have been derived microscopically from the deformed potentials as ground state expectations of the Q_{20} operator. We can compare again with the results from relativistic mean field calculations of Ref. [25]: $Q_{p(\text{rel})}(^{76}\text{Ge}) = 111.4$ fm^2 and $Q_{p(\text{rel})}(^{76}\text{Se}) = -146.8$ fm^2. These relativistic results are in perfect accordance with our calculated results. They can also be compared with experimental intrinsic quadrupole moments from Ref. [26]. The empirical intrinsic moments are derived from the laboratory moments assuming a well defined deformation. These values are shown in Table I in the first place: $Q_{p(\text{exp})}(^{76}\text{Ge}) = 66(21)$ fm^2 and $Q_{p(\text{exp})}(^{76}\text{Se}) = 119(25)$ fm^2. Experimental quadrupole moments can also be derived [27] from the experimental values of $B(E2)$ strengths, although in this case the sign cannot be extracted. Assuming that the intrinsic electric quadrupole moments are given by $Q = \sqrt{16\pi B(E2)/5e^2}$, then $|Q_{p(\text{exp})}|(^{76}\text{Ge}) = 164(24)$ fm^2 and $|Q_{p(\text{exp})}|(^{76}\text{Se}) = 205(24)$ fm^2.

IV. GAMOW-TELLER STRENGTH DISTRIBUTIONS

In this section we show and discuss the Gamow-Teller strength distributions obtained from different choices of the deformed mean fields and residual interactions.

As a general rule, the following figures showing the GT strength distributions are plotted versus the excitation energy of daughter nucleus. The distributions of the GT strength have been folded with Breit-Wigner functions of 1 MeV width to facilitate the comparison among the various calculations, so that the original discrete spectrum is transformed into a continuous profile. These distributions are given in units of $g_A^2/4\pi$ and one should keep in mind that a quenching of the g_A factor, typically $g_{A,\text{eff}} = (0.7–0.8)\, g_{A,\text{free}}$, is expected on the basis of the observed quenching in charge exchange reactions.

First of all, we discuss in Figs. 2 and 3, the dependence of the GT strength distributions on the deformed quasiparticle mean field of ^{76}Ge and ^{76}Se, respectively. To make the discussion meaningful we show the results obtained at the two-quasiparticle level without including the spin-isospin residual interactions. In these figures we can see the $B(\text{GT}_-)$ and $B(\text{GT}_+)$ strength distributions in the upper and lower panels, respectively. One should notice that the relevant strength distributions for the double β decay of ^{76}Ge, as can be seen schematically in Fig. 4, are the $B(\text{GT}_-)$ distribution of the parent ^{76}Ge and the $B(\text{GT}_+)$ distribution of daughter ^{76}Se, but for completeness we show both distributions for each nucleus. Solid lines in Figs. 2 and 3 correspond to the results obtained from the Skyrme force SG2 within a HF scheme, dashed lines correspond to the results obtained with the WS potential. The deformation of the mean fields are as indicated in Table I, using the prolate shape in ^{76}Se. Pairing correlations are included in HF and WS cases in a similar way with the gap parameters for neutrons and protons mentioned earlier. Then, the only source of discrepancy between
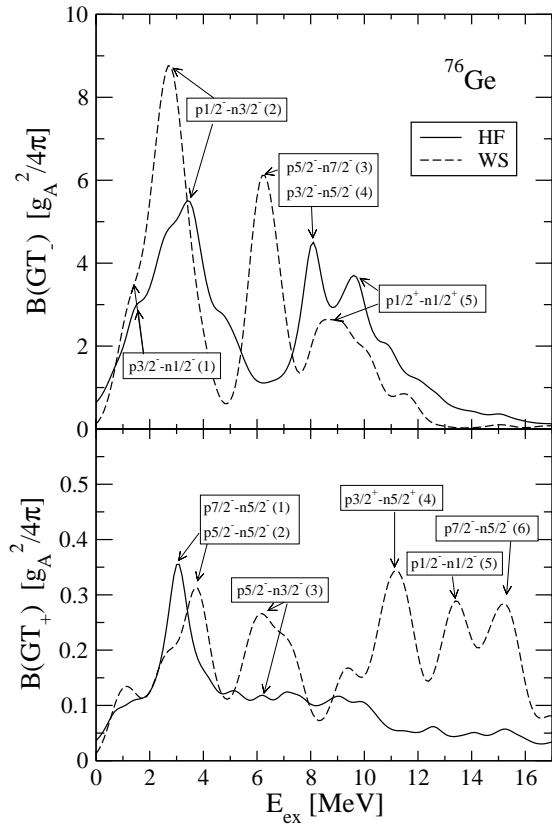
FIG. 2. Gamow-Teller $B(GT_-)$ and $B(GT_+)$ strength distributions $[g_A^2/4\pi]$ in ^{76}Ge plotted as a function of the excitation energy of the daughter nucleus. We compare results of HF(SG2)+BCS (solid line) and WS+BCS (dashed line) approximations for the prolate minima.

HF and WS comes from the different single-particle wave functions and energies.

In general, we observe that WS and HF produce a similar structure of three peaks in the $B(GT_-)$ profiles of ^{76}Ge and ^{76}Se, although the WS results are somewhat displaced to lower energies with respect to the HF peaks. The strengths contained in the peaks are also comparable. In the case of the $B(GT_+)$ distributions, we first observe the different scale, which is about one order of magnitude lower than the $B(GT_-)$ scale. This is a consequence of the Pauli blocking. We can see from Eq. (15) that while the occupation amplitudes $u's$ and $v's$ favor M_- strengths, they are very small factors in M_+ strengths when connecting similar proton and neutron states. The difference between total $B(GT_-)$ and $B(GT_+)$ strengths [Ikeda sum rule (16), which is fulfilled in our calculations] is a large number $3(N-Z)=36$ in ^{76}Ge and $3(N-Z)=24$ in ^{76}Se, reflecting the different magnitude of the $B(GT_-)$ and $B(GT_+)$ strengths shown in Figs. 2 and 3.

The profiles of the $B(GT_+)$ distributions with WS and HF present some discrepancies that are amplified by the scale. Particularly remarkable is the large strength produced by WS in the region of high excitation energies in ^{76}Ge that we discuss later in terms of the single-particle wave functions.

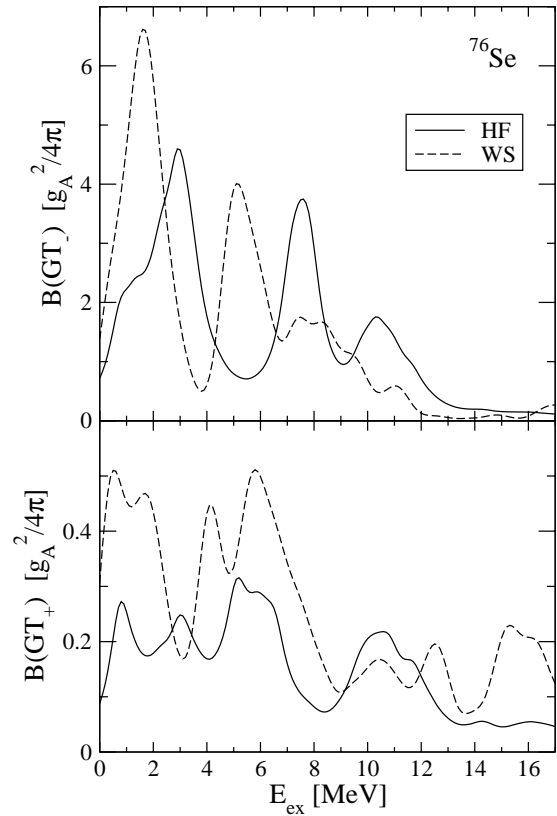In order to clarify the origin of the various peaks in the

FIG. 3. Same as in Fig. 2, but for ^{76}Se.

strength distributions we have added in Fig. 2 labels showing some of the leading transitions generating the strength. The labels stand for $pK^\pi - nK'^\pi$ of the orbitals connected by the spin operator in Eq. (11) and a number that identifies the transition. In both cases, $B(GT_-)$ and $B(GT_+)$, the same type of transitions are connected by the GT operator but the occupation probabilities, weighting the matrix elements, enhance or reduce them accordingly. We can see from Fig. 2 that the structure of the profiles in both WS and HF is gen-
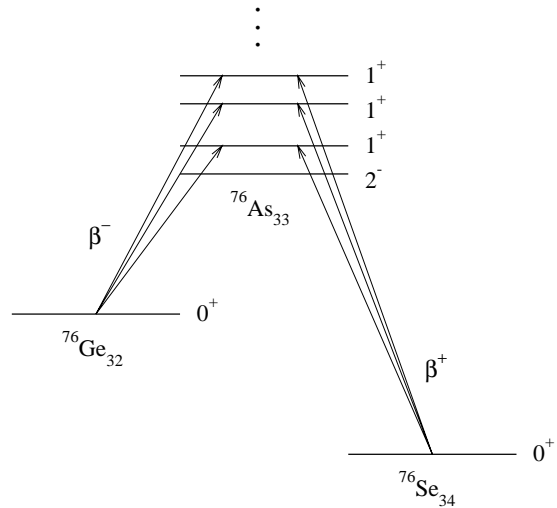

FIG. 4. Schematic picture of the GT β^- (β^+) decay of ^{76}Ge (^{76}Se) into ^{76}As.
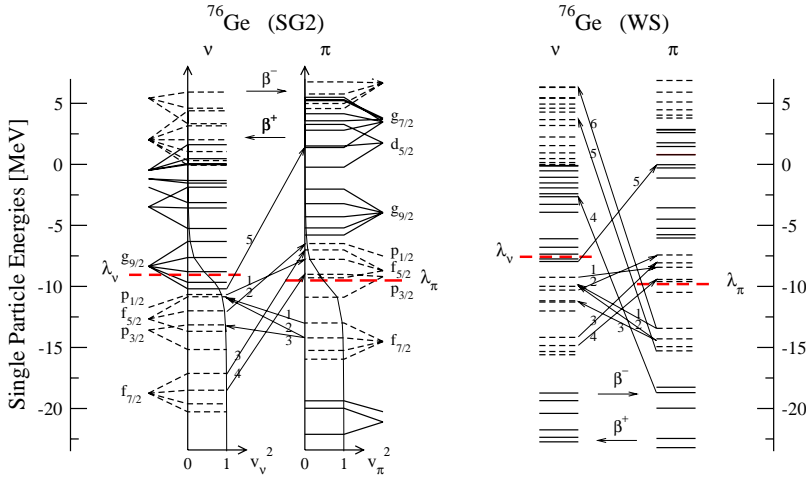
FIG. 5. Hartree-Fock and Woods-Saxon single-particle energies for protons and neutrons in ^{76}Ge.

erated by the same type of GT transitions.

This can be further illustrated by looking at Fig. 5, where we show the single-particle energies for protons and neutrons obtained in HF(SG2) and WS in ^{76}Ge. In the left part of the figure corresponding to the HF calculation we have plotted the occupation probabilities v_ν^2 and v_π^2 and the Fermi energies λ_ν and λ_π. We can also see for completeness the spherical levels labeled by their ℓ_j values. We have indicated by arrows the most relevant Gamow-Teller transitions in the β^- and β^+ directions that are labeled by the same numbers used in Fig. 2 to identify the peaks. To be more precise, we can see in Table II the correspondence between these labels and the transitions connecting the proton and neutron states using the asymptotic quantum number notation $[Nn_z\Lambda]K^\pi$.

Now, looking at Fig. 2, we can understand that the two first peaks in $B(GT_-)$ are generated mainly by transitions between neutrons and protons dominated by contributions within the $N=3$ shell and that the third peak is generated by transitions between neutrons and protons with main contributions coming from the $N=4$ shell. The different energies of the peaks are due to the different concentration of energy levels in HF and WS.

In the case of $B(GT_+)$, the strength below 8 MeV is mainly generated by transitions within the $N=3$ shells. Beyond 8 MeV, the strength, which is negligible in HF, is generated by transitions between the proton shell $N=2$ and the neutron shell $N=4$ as well as between the proton shell $N=3$ and the neutron shell $N=5$, always understood as the main components of the wave functions. Then, very deep

inside protons ($v_p=1$) are connected with very unoccupied neutron states ($u_n=1$), giving rise to maximum occupation factors. The different behavior in this high-energy region between HF and WS is therefore due, other factors such as deformation and occupations being equal, to the structure of the deformed orbitals.

To illustrate the role of the different single-particle wave functions in the development of the peak structure, we consider in detail the case of the last peak observed in the $B(GT_+)$ distribution of the WS potential. As we can see, it is mainly due to a transition between the proton state [303] in the $N=3$ shell with $K^\pi=7/2^-$ and the neutron state [523] in the $N=5$ shell with $K^\pi=5/2^-$. The structure of the single-particle wave functions, according to the expansion in Eq. (1), of these two states in the cases of HF and WS can be seen in Table III. With these coefficients we can construct the matrix elements in Eq. (12). The resulting strength is almost two orders of magnitude in favor of WS, which explains the huge discrepancy observed between WS and HF in the higher-energy domain.

Nevertheless, these discrepancies are smaller in the case of the $B(GT_+)$ of ^{76}Se, which is the relevant branch for the double β decay of the parent nucleus ^{76}Ge.

Figures 6 and 7 contain the strength distributions obtained from QRPA calculations for ^{76}Ge and ^{76}Se, respectively. The data in Fig. 6 are from Ref. [28] and were obtained from charge exchange ^{76}Ge$(p,n)^{76}$As reactions. The thick line in Fig. 6 corresponds to these data folded by the same procedure used for the theoretical results. The data in Figs. 7 and 8 are from Ref. [29] and were obtained from charge exchange ^{76}Se$(n,p)^{76}$As reactions.

The coupling constants of the *ph* and *pp* residual interactions used in Figs. 6–8 are from Ref. [7] in the case of WS. In our case with $A=76$, these parameters are $\chi_{GT}^{ph}=0.25$ MeV and $\kappa_{GT}^{pp}=0.027$ MeV. In the case of the HF calculations with the Skyrme forces Sk3 and SG2, better agreement with the measured location of the $B(GT_-)$ resonance in ^{76}Ge is obtained with a somewhat smaller value of the *ph* strength. The curves shown in Figs. 6–8 for the HF results have been obtained using $\chi_{GT}^{ph}=0.16$ MeV and the same $\kappa_{GT}^{pp}=0.027$ MeV.

TABLE II. Correspondence of the labels used in Figs. 2 and 5 with the asymptotic quantum numbers notation $[Nn_z\Lambda]K^\pi$.

	β^-	β^+
(1)	$\nu[301]1/2^- \rightarrow \pi[301]3/2^-$	$\pi[303]7/2^- \rightarrow \nu[303]5/2^-$
(2)	$\nu[301]3/2^- \rightarrow \pi[301]1/2^-$	$\pi[312]5/2^- \rightarrow \nu[303]5/2^-$
(3)	$\nu[303]7/2^- \rightarrow \pi[303]5/2^-$	$\pi[312]5/2^- \rightarrow \nu[312]3/2^-$
(4)	$\nu[312]5/2^- \rightarrow \pi[312]3/2^-$	$\pi[202]3/2^+ \rightarrow \nu[413]5/2^+$
(5)	$\nu[420]1/2^+ \rightarrow \pi[440]1/2^+$	$\pi[330]1/2^- \rightarrow \nu[530]1/2^-$
(6)		$\pi[303]7/2^- \rightarrow \nu[523]5/2^-$

TABLE III. Main coefficients C_α^i in the expansion of Eq. (1) for the proton state [303] with $K^\pi = 7/2^-$ and the neutron state [523] with $K^\pi = 5/2^-$. This is the main contribution to the peak at 15 MeV in the $B(GT_+)$ strength distribution of ^{76}Ge with the Woods-Saxon potential. The basis states are labeled by $|Nn_z\Lambda\rangle$ quantum numbers. The table contains also the contributions from these basis states to the spin matrix elements in Eqs. (11) and (12).

		$|303\rangle$	$|503\rangle$	$|523\rangle$	$|703\rangle$	$|723\rangle$	$|903\rangle$
$7/2^-$ proton							
	HF(SG2)	-0.9742	0.2204	-0.0061	0.0219	-0.0272	0.0122
	WS	0.9876	-0.1400	0.0563	-0.0233	0.0107	-0.0295
$5/2^-$ neutron							
	HF(SG2)	0.1369	0.5933	-0.5031	-0.3928	0.2349	0.2385
	WS	-0.2397	-0.5173	0.5049	0.3794	-0.2596	-0.2056
Contribution to $\Sigma_K^{\nu\pi}$							
	HF(SG2)	-0.1333	0.1308	0.0031	-0.0107	-0.0064	0.0029
	WS	-0.2367	0.0724	0.0284	-0.0088	-0.0028	0.0061

In Fig. 6 we have used the prolate deformations for ^{76}Ge given in Table I. We can see that WS follows the structure of the experimental $B(GT_-)$ strength distribution with two peaks at low energies ($E_{ex}=5$ and 8 MeV) and the resonance at 11 MeV. The HF calculations produce also a few peaks at low excitation energies and a resonance between 10

and 13 MeV. We can see that the structure of the strength distributions is qualitatively similar for the two Skyrme forces and that the difference with the WS curves can be traced back to the discrepancies found at the two-quasiparticle level.

Figure 7 contains similar calculations for ^{76}Se. The coupling strengths of the residual forces are as indicated for ^{76}Ge. The results in the HF cases are obtained with the oblate deformation of ^{76}Se that produces the absolute minimum of the energy and agrees better with the experimental quadrupole moment. In general, comparison with experiment is
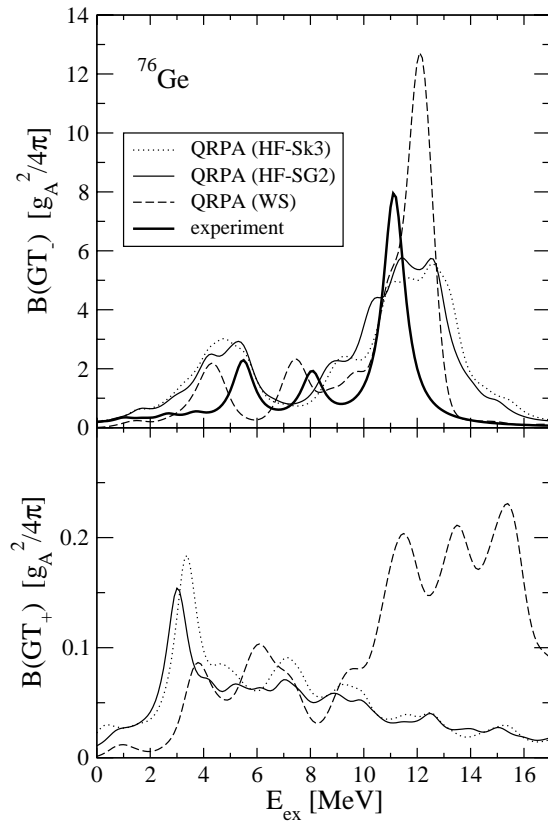

FIG. 6. Gamow-Teller $B(GT_-)$ and $B(GT_+)$ strength distributions $[g_A^2/4\pi]$ in ^{76}Ge plotted as a function of the excitation energy of the daughter nucleus. We compare QRPA results of HF(SG2) (solid lines), HF(Sk3) (dotted lines), and WS (dashed lines). Deformations and coupling strengths of the residual interactions are given in the text. Experimental data (thick solid lines) are from Ref. [28].
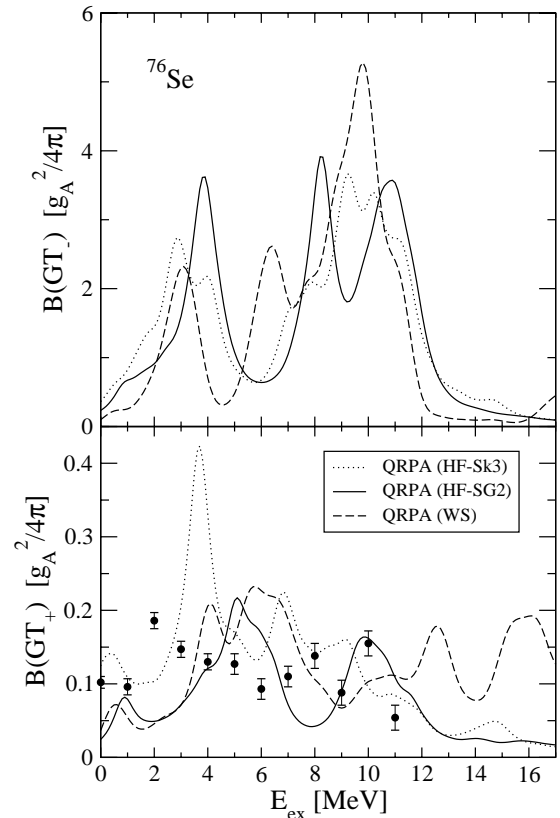

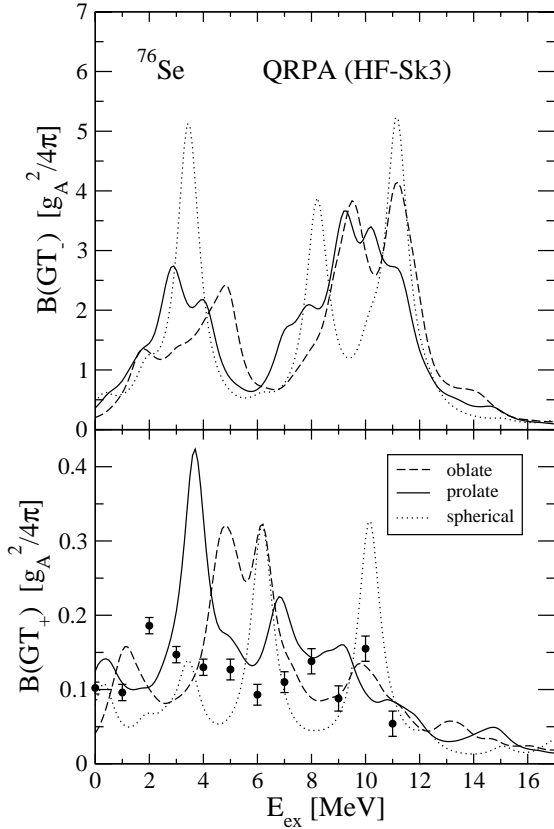FIG. 7. Same as in Fig. 6, but for ^{76}Se. Data are from Ref. [29].

FIG. 8. QRPA Gamow-Teller $B(GT_-)$ and $B(GT_+)$ strength distributions in ^{76}Se. The calculations correspond to the force Sk3 for spherical (dotted line), prolate (solid line), and oblate (dashed line) shapes. Data are from Ref. [29].

TABLE IV. Total Gamow-Teller strength in ^{76}Se calculated with the force Sk3. Results correspond to β^+ and β^- strengths for the oblate, spherical, and prolate shapes calculated in 2qp and QRPA approximations. All the GT strength contained below an excitation energy of 60 MeV has been included.

	Oblate		Spherical		Prolate	
	β^+	β^-	β^+	β^-	β^+	β^-
RPA	2.420	26.331	1.846	25.765	2.599	26.524
2qp	4.387	28.298	3.816	27.736	4.971	28.892

sizable differences between the GT strength distributions corresponding to different shapes.

We can see in Fig. 8 the GT strength distributions in ^{76}Se obtained from spherical, prolate, and oblate shapes. They correspond to QRPA calculations performed with the HF basis obtained with the force Sk3. In the spherical case, the only possible transitions (see Fig. 5) are those connecting spherical ℓ_j partners with $\Delta\ell = 0$, $\Delta j = 0,1$, in allowed approximation. Therefore, there is GT strength only at a few excitation energies. The strength we observe in Fig. 8 is the result of the folding procedure performed at these energies. On the other hand, in the deformed cases we can observe a stronger fragmentation, which is the result of all possible connections among the deformed states (see Fig. 5). Thus, the spherical peaks become broader when deformation is present.

We can see in Table IV the total GT strengths in ^{76}Se contained below an energy cut of 60 MeV. We show the results obtained for β^+ and β^- strengths with oblate, spherical, and prolate shapes. The Ikeda sum rule $3(N-Z) = 24$, is fulfilled at this energy cut within a 0.3% accuracy. We can see from Table IV that deformation increases both β^+ and β^- strengths in a similar amount in order to preserve the Ikeda sum rule ($\beta^- - \beta^+$). We also show for comparison the results obtained in 2qp approximation. We can see the reduction of the strength introduced by the QRPA correlations, which is again similar in absolute terms for β^+ and β^- strengths in order to keep the Ikeda sum rule conserved in QRPA. Since the β^- strength is much larger than the β^+ strength, the relative effect of the QRPA correlations is much stronger for β^+, where the total strength is reduced by 50%.

Comparing the results for ^{76}Se obtained at different deformations with the self-consistent mean fields (HF with Sk3) in Fig. 8 and Table IV, we see that there is a strong dependence on deformation in the strength distributions as a function of the energy. However, the total strength does not depend so much on deformation. There is an increase of a few percent in going from the spherical to the oblate and prolate shapes. The latter observation enters in contradiction with SU(3) and shell model calculations by previous authors [30] on the dependence on deformation of the GT strengths in ^{20}Ne and ^{44}Ti. We think that this is due to the much larger and richer single-particle basis used in the present calculations. In our case each single-particle state contains mixtures from many harmonic oscillator shells (up to $N=10$), while in the above mentioned calculations [30], the single-particle basis is restricted to a single harmonic oscillator major shell

reasonable and should not be stressed too much since, as stated in Ref. [29], the experimental results, especially above 6 MeV, must be considered to be of a qualitative nature only.

The role of the residual interactions on the GT strengths was already studied in Ref. [8], where it was shown that the repulsive ph force introduces two types of effects. A shift of the GT strength to higher excitation energies with the corresponding displacement of the position of the GT resonance and a reduction of the total GT strength. The residual pp, being an attractive force, shifts the strength to lower excitation energies, reducing the total GT strength as well. Also shown in Ref. [8] was the effect of the BCS correlations on the GT strength distribution. The main effect of pairing correlations is to create new transitions that are forbidden in the absence of such correlations. The main effect of increasing the Fermi diffuseness is to smooth out the profile of the GT strength distribution, increasing the strength at high energies and decreasing the strength at low energies.

The role of deformation was also studied in Ref. [8], showing that the GT strength distributions corresponding to deformed nuclear shapes are much more fragmented than the corresponding spherical ones, as it is clear because deformation breaks down the degeneracy of the spherical shells. It was also shown that the crossing of deformed energy levels that depends on the magnitude of the quadrupole deformation as well as on the oblate or prolate character, may lead to

(the sd shell in ^{20}Ne and the fp shell in ^{44}Ti). On the other hand, one may question whether in the deformed cases the total strengths calculated here may contain spurious contributions from higher angular momentum components in the initial and final nuclear wave functions. Since the matrix elements of the transition operator, which is a dipole tensor operator, are taken between the states considered in the laboratory frame [see Eq. (14)], the effect of angular momentum projection is to a large extent taken into account. We have calculated an upper bound to such contributions using angular momentum projection techniques [31]. We find that this upper bound is less than 1% ($\sim \langle J_\perp^2 \rangle^{-2}$, with $\langle J_\perp^2 \rangle = 19$ for the oblate shape in ^{76}Se). Thus, exact angular momentum projection would not wash out the small increase of the total strength with deformation.

V. CONCLUDING REMARKS

We have studied the GT strength distributions for the two decay branches β^- and β^+ in the double β decay of ^{76}Ge. This has been done within a deformed QRPA formalism, which includes ph and pp separable residual interactions. The quasiparticle mean field includes pairing correlations in BCS approximation and it is generated by two different methods, a deformed HF approach with Skyrme interactions and a phenomenological deformed WS potential. One difference is that with HF and Sk3 we get the minimum and stable deformation for ^{76}Se to be oblate, while the prolate minimum is comparable to that obtained with WS and is higher in energy.

We have studied the similarities and differences observed in the GT strength distributions with these two methods.

Among the similarities we can mention the structure of peaks found in the strength distributions and among the differences the displacement in the excitation energies found between HF and WS results. This discrepancy has its origin in the structure of the single-particle wave functions and energies generated by the deformed mean fields. This also implies that different mean fields require different residual interactions to reproduce the experimental GT resonances.

Therefore, in order to obtain reliable GT strength distributions and consequently reliable estimates for double β-decay half-lives, it is important to have not only the proper residual interactions but also a good deformed single-particle basis as a starting point. In the case of HF we have seen that standard Skyrme forces, such as SG2 or Sk3, give a good description of the GT strength distributions, provided the proper residual interactions are included. Even though the self-consistent HF approach is a more sophisticated type of calculation, the deformed WS potential produces comparable results when the parameters of the potential and the residual interactions for a given mass region are chosen properly.

There is work in progress to extend these calculations to the double β-decay process studying the dependence on deformation of the half-lives.

[1] J. Suhonen and O. Civitarese, Phys. Rep. **300**, 123 (1998); A. Faessler and F. Šimkovic, J. Phys. G **24**, 2139 (1998); H. V. Klapdor-Kleingrothaus, *Sixty Years of Double Beta Decay* (World Scientific, Singapore, 2001).

[2] J.A. Halbleib and R.A. Sorensen, Nucl. Phys. **A98**, 542 (1967).

[3] P. Vogel and M.R. Zirnbauer, Phys. Rev. Lett. **57**, 3148 (1986); D. Cha, Phys. Rev. C **27**, 2269 (1987); T. Tomoda and A. Faessler, Phys. Lett. B **199**, 475 (1987); K. Muto, E. Bender, and H.V. Klapdor, Z. Phys. A **334**, 177 (1989).

[4] J. Hirsch, E. Bauer, and F. Krmpotić, Nucl. Phys. **A516**, 304 (1990); A.A. Raduta, A. Faessler, S. Stoica, and W.A. Kaminski, Phys. Lett. B **254**, 7 (1991); J. Toivanen and J. Suhonen, Phys. Rev. Lett. **75**, 410 (1995); J. Schwieger, F. Šimkovic, and A. Faessler, Nucl. Phys. **A600**, 179 (1996); A.A. Raduta, M.C. Raduta, A. Faessler, and W.A. Kaminski, *ibid.* **A634**, 497 (1998); A.A. Raduta, F. Šimkovic, and A. Faessler, J. Phys. G **26**, 793 (2000).

[5] J. Krumlinde and P. Möller, Nucl. Phys. **A417**, 419 (1984).

[6] P. Moller and J. Randrup, Nucl. Phys. **A514**, 1 (1990).

[7] H. Homma, E. Bender, M. Hirsch, K. Muto, H.V. Klapdor-Kleingrothaus, and T. Oda, Phys. Rev. C **54**, 2972 (1996).

[8] P. Sarriguren, E. Moya de Guerra, A. Escuderos, and A.C. Carrizo, Nucl. Phys. **A635**, 55 (1998); P. Sarriguren, E. Moya de Guerra, and A. Escuderos, *ibid.* **A658**, 13 (1999); **A691**, 631 (2001); Phys. Rev. C **64**, 064306 (2001).

[9] J. Engel, M. Bender, J. Dobaczewski, W. Nazarewicz, and R. Surnam, Phys. Rev. C **60**, 014302 (1999); M. Bender, J. Dobaczewski, J. Engel, and W. Nazarewicz, *ibid.* **65**, 054322 (2002).

[10] A.A. Raduta, A. Faessler, and D.S. Delion, Nucl. Phys. **A564**, 185 (1993); Phys. Lett. B **312**, 13 (1993); **A617**, 176 (1997).

[11] F. Šimkovic, L. Pacearescu, and A. Faessler (unpublished).

[12] H. Flocard, P. Quentin, and D. Vautherin, Phys. Lett. **46B**, 304 (1973); P. Quentin and H. Flocard, Annu. Rev. Nucl. Part. Sci. **28**, 253 (1978); P. Bonche, H. Flocard, P.H. Heenen, S.J. Krieger, and M.S. Weiss, Nucl. Phys. **A443**, 39 (1985).

[13] Y. Tanaka, Y. Oda, F. Petrovich, and R.K. Sheline, Phys. Lett. **83B**, 279 (1979).

[14] R. Nojarov, A. Faessler, P. Sarriguren, E. Moya de Guerra, and M. Grigorescu, Nucl. Phys. **A563**, 349 (1993); P. Sarriguren, E. Moya de Guerra, R. Nojarov, and A. Faessler, J. Phys. G **20**, 315 (1994); J.M. Udias, R. Nojarov, and A. Faessler, *ibid.* **23**, 1673 (1997).

[15] M. Beiner, H. Flocard, N. Van Giai, and P. Quentin, Nucl. Phys. **A238**, 29 (1975).

[16] N. Van Giai and H. Sagawa, Phys. Lett. **106B**, 379 (1981).

[17] P. Sarriguren, E. Moya de Guerra, and R. Nojarov, Phys. Rev. C **54**, 690 (1996); Z. Phys. A **357**, 143 (1997).

[18] D. Vautherin and D.M. Brink, Phys. Rev. C **5**, 626 (1972); D. Vautherin, *ibid.* **7**, 296 (1973).

[19] M. Vallières and D.W.L. Sprung, Can. J. Phys. **56**, 1190 (1978).

[20] G. Audi and A.H. Wapstra, Nucl. Phys. **A595**, 409 (1995); G. Audi, O. Bersillon, J. Blachot, and A.H. Wapstra, *ibid.* **A624**, 1 (1997).

[21] M. Hirsch, A. Staudt, K. Muto, and H.V. Klapdor-Kleingrothaus, Nucl. Phys. **A535**, 62 (1991); K. Muto, E. Bender, and H.V. Klapdor, Z. Phys. A **333**, 125 (1989); K. Muto, E. Bender, T. Oda, and H.V. Klapdor-Kleingrothaus, *ibid.* **341**, 407 (1992).

[22] A. Bohr and B. Mottelson, *Nuclear Structure* (Benjamin, New York, 1975).

[23] H. Flocard, P. Quentin, A.K. Kerman, and D. Vautherin, Nucl. Phys. **A203**, 433 (1973).

[24] H. de Vries, C.W. de Jager, and C. de Vries, At. Data Nucl. Data Tables **36**, 495 (1987); G. Fricke, C. Bernhardt, K. Heilig, L.A. Schaller, L. Schellenberg, E.B. Shera, and C.W. de Jager, *ibid.* **60**, 177 (1995).

[25] G.A. Lalazissis, S. Raman, and P. Ring, At. Data Nucl. Data Tables **71**, 1 (1999).

[26] P. Raghavan, At. Data Nucl. Data Tables **42**, 189 (1989); N. J. Stone (unpublished).

[27] S. Raman, C.H. Malarkey, W.T. Milner, C.W. Nestor, Jr., and P.H. Stelson, At. Data Nucl. Data Tables **36**, 1 (1987).

[28] R. Madey, B.S. Flanders, B.D. Anderson, A.R. Baldwin, J.W. Watson, S.M. Austin, C.C. Foster, H.V. Klapdor, and K. Grotz, Phys. Rev. C **40**, 540 (1989).

[29] R.L. Helmer *et al.*, Phys. Rev. C **55**, 2802 (1997).

[30] N. Auerbach, D.C. Zheng, L. Zamick, and B.A. Brown, Phys. Lett. B **304**, 17 (1993); D. Troltenier, J.P. Draayer, and J.G. Hirsch, Nucl. Phys. **A601**, 89 (1996).

[31] E. Moya de Guerra, Phys. Rep. **138**, 293 (1986).